Supplement Material

Sirtuin SIRT1 retards hyperphosphatemia-induced calcification of vascular smooth muscle cells

Methods

Aortic calcification in renal failure rats

Renal failure was induced in rats by a 0.75% adenine-containing diet as previously described.[28] Twelve-week-old male Wistar rats (Nippon Clea Inc., Japan) were pair-fed standard CE-2 chow (containing 1.2% calcium and 0.6% phosphorus; Nippon Clea Inc.) in the control group or CE-2 chow containing 0.75% adenine (Sigma) in the renal failure group for 4 weeks. Then, the diet was returned to normal chow for an additional 4 weeks. After induction of renal failure for 8 weeks in total, the rats were sacrificed to collect samples. After perfusion with saline at a constant, nonpulsatile pressure of 100 mmHg, the aorta was immediately embedded in OCT compound frozen section and sequentially cut into cross-sections with 5-μm thickness from each part of the aorta. To detect calcification in the aortic wall, each cross-section was subjected to von-Kossa staining to demonstrate mineralization. The calcified area and number of

SAβ-gal-positive cells in the cross-section were measured by image analysis software (ImageJ, Scion Image, Maryland, USA). All procedures and animal care were in accordance with the Guide for the Care and Use of Laboratory Animals of the University of Tokyo.

Induction of SMC calcification

Primary human aortic SMC (HASMC), derived from the internal thoracic artery (Clonetics), were treated with a pathological concentration of inorganic phosphate (Pi) in culture medium. To set up the calcification medium, a mixed solution of Na_2HPO_4 and NaH_2PO_4 whose pH was adjusted to 7.4 was added to serum-supplemented DMEM to final doses of up to 3.2 mmol/L as previously described.[29] To quantitatively measure Pi-induced calcification, two distinct experiments, (1) intracellular calium (Ca) deposition as determined by *o*-cresolphthalein complexone method and (2) visualization of mineralization as determined by von-Kossa staining, were performed as previously described.[28] We have previously confirmed that excessive Pi stimulation dose- and time-dependently induced calcium deposition in HASMC, whereas a normal Pi dose (1.4 mmol/L), equivalent to the human physiological level of serum phosphate, did not.[29]

Senescence-associated β-galactosidase (SAβ-gal) staining

To assess senescent changes in the phenotype of cultured HASMC or aortic medial cells of rats with/without renal failure, staining for senescence-associated β-galactosidase (SAβ-gal), a well-established biomarker of cellular senescence, was performed at pH 6.0, as opposed to endogenous lysosomal enzyme detected at pH 4.0 in normal cells, as previously described.[30] Numbers of SAβ-gal-positive cells were quantitatively counted in the aortic wall or cultured HASMC. As a positive control in *in vitro* experiments, angiotensin II (AngII) was used to induce transition to a senescent phenotype in HASMC.

Knockdown of SIRT1 or p21 by small interfering RNA

HASMC were transfected with 200 pmol/L small interfering RNA (siRNA) for SIRT1 (GAT GAA GTT GAC CTC CTC A and TGA AGT GCC TCA GAT ATT A, Santa Cruz Biotechnology) or control (Cntl) using silMPORTER (Upstate). In addition, knockdown of $p21^{WAF1/CIP1}$ was performed using 100 to 200 pmol/L siRNA for p21 (CGA CUG UGA UGC GCU AAU G, CCU AAU CCG CCC ACA GGA A, CGU CAG AAC CCA UGC GGC A, and AGA CCA GCA UGA CAG AUU U) by the same

method. To inhibit p21 expression effectively and completely, four kinds of sequences of p21 siRNA were used. HASMC were treated simultaneously with these siRNAs at the start of Pi stimulation.

Western blot and SDS-PAGE

Protein expression was assessed by Western blot analysis with chemiluminescence detection. SIRT1 was detected using a rabbit polyclonal anti-SIRT1 antibody (Abcam), and p53, acetylated p53 (Ac-p53; Lys-382), acetylated histone-3 (Ac-H3), p21, caldesmon and β-tubulin were detected with monoclonal antibodies (Santa Cruz Biotechnology). The expression levels of Ac-p53 and Ac-H3 were used to reflect SIRT1 activity as a deacetylase. Caldesmon was used to reflect a lineage marker of SMC differentiation.

Real-time PCR analysis: Osteoblastic markers

Primer sequences were as follows:

ALP; (forward) ACCATTCCCACGTCTTCACATTTG,

(reverse) AGACATTCTCTCGTTCACCGCC,

Runx-2/Cbfa-1; (forward) TCTGGCCTTCCACTCTCAGT,

(reverse) GACTGGCGGGGTGTAAGTAA,

SIRT1; (forward) CCTGACTTCAGGTCAAGGGATGGTA,

(reverse) CTGATTAAAAATATCTCCTCGTACAG,

β-actin; (forward) CTGGAACGGTGAAGGTGACA,

(reverse) AAGGGACTTCCTGTAACAATGC.

Materials

Angiotensin II (AngII) was used to induce senescent phenotypic change in cultured HASMC as a positive control. To inhibit activity of Na-dependent phosphate cotransporter (NPC) stimulated by treatment with exogenous Pi, phosphonoformic acid (PFA; SIGMA), a chemical inhibitor, was used. Sirtinol (a chemical inhibitor; Calbiochem) or resveratrol (an activator of SIRT1; WAKO) was used for modulation of SIRT1 activity. Localization of SIRT1 in HASMC was detected using its antibody (Santa Cruz: sc-15404).

Immunohistological staining

To address a difference in senescent induction by Pi or AngII, the localization of SIRT1 in HASMC was compared using immunohistological assessment. SIRT1 specific

antibody showed localization and its translocation in HSMC before or after stimulation of Pi alone (2.6 mM) or AngII alone (10 pmol/L). Nucleus was detected by DAPI stain.

Statistical analysis

All results are presented as mean ± standard error (SE). Differences between the groups were analyzed using ANOVA, followed by Fisher's PLSD test. A value of $P < 0.05$ was considered to be significant. All *in vitro* experiments were performed at least three times.

Figure legends

Supplemental figure 1. Deterioration of osteoblastic transition by SIRT1 knockdown under high-dose Pi stimulation

The effect of SIRT1 knockdown on osteoblastic markers, Runx2 and ALP, in the condition of normal Pi or high-dose Pi was examined. Complete knockdown of SIRT1 showed significantly augmented expression of both osteoblastic markers, Runx2 and ALP, in a high-dose Pi condition; however, augmentation was not found in a normal Pi condition. These data suggest that intracellular Pi influx by Pi stimulation is essential to

induce SMC calcification in association with osteoblastic phenotypic change, and the osteoblastic transition may be correlated with NPC, a cotransporter of Pi.

Supplemental figure 2. Translocation of SIRT1 in HASMC is induced by Pi, but not AngII.

To address a difference in senescent induction by Pi or AngII, immunohistological assessment of SIRT1 in HASMC was examined. SIRT1 was predominantly localized in nucleus without Pi. Dynamic translocation of SIRT1 to cytoplasm was observed after Pi stimulation (2.6 mM) for 24 hr and its expression disappeared in both areas on day 6. In contrast, AngII alone (10 pmol/L) did not show the dynamic translocation. SIRT1 siRNA shows complete knockdown of SIRT1 expression. DAPI shows nuclear stain.

Supplement Material Figure I

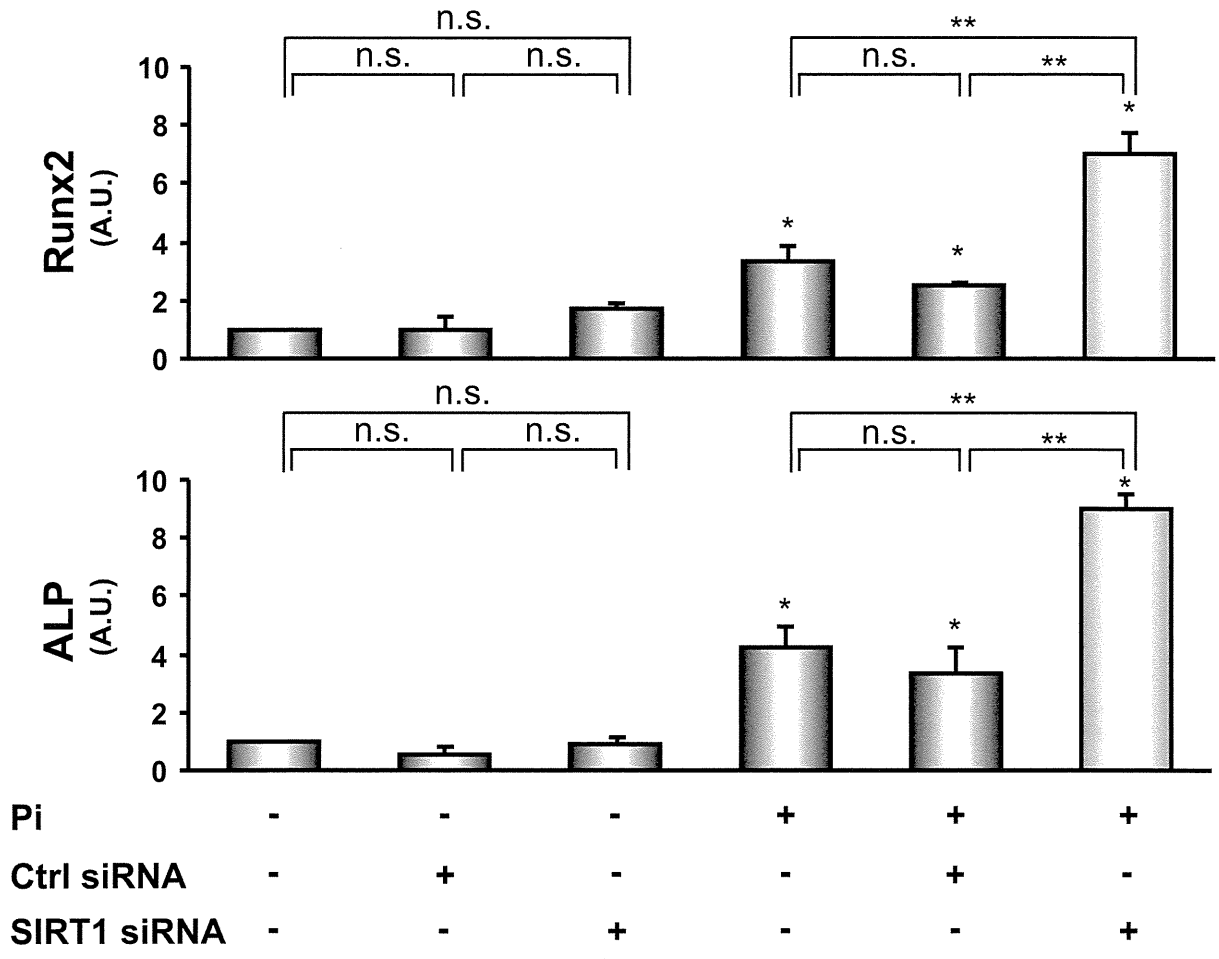

Supplement Material Figure Ⅱ

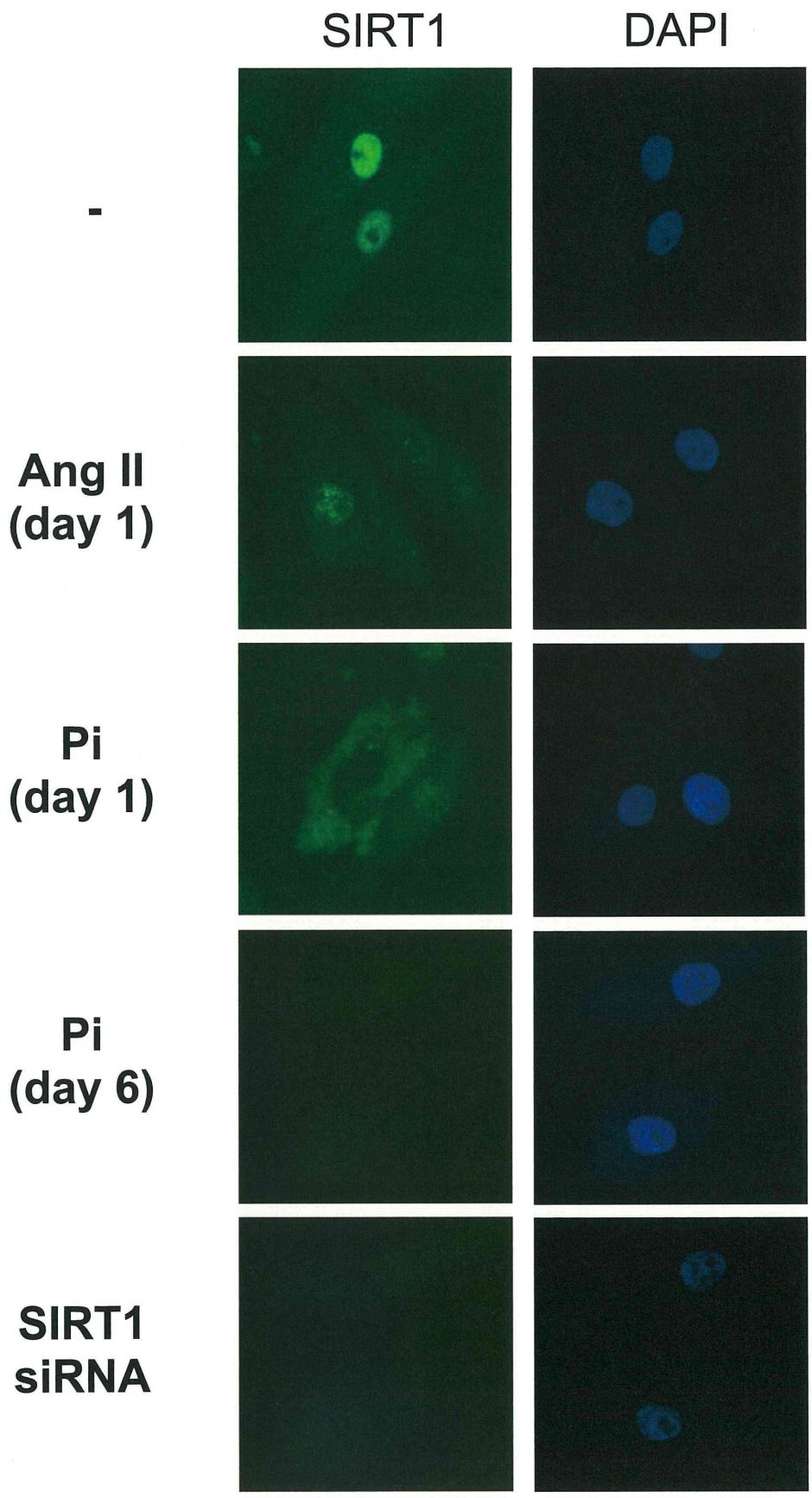

Bruno Fantino, MD, PhD
Medical School
University of Angers
UNAM
Angers, France
Department of Geriatrics
Angers University Hospital
Angers, France

Laure De Decker, MD, MS
Medical School
University of Nantes
UNAM
Nantes, France
Department of Geriatrics
Nantes University Hospital
Nantes, France

Olivier Beauchet, MD, PhD
Cédric Annweiler, MD, PhD
Medical School
University of Angers
UNAM
Angers, France
Department of Geriatrics
Angers University Hospital
Angers, France

ACKNOWLEDGMENTS

The authors wish to thank Angers University Hospital for technical support.

Conflict of Interest: Prof. Beauchet serves as an unpaid consultant for Ipsen Pharma company and as a board member for Gériatrie, Psychologie et Neuropsychiatrie du Vieillissement. He has no relevant financial interest in this manuscript. Dr. Annweiler serves as an unpaid consultant for Ipsen Pharma Company. He has no relevant financial interest in this manuscript.

Author Contributions: Annweiler had full access to the data in the study and takes responsibility for the integrity of the data and the accuracy of the data analyses. Study concept and design: Annweiler and Beauchet. Acquisition of data: Calès, Redureau, and Abraham. Analysis and interpretation of data: Abraham, Calès, Redureau, Annweiler, and Beauchet. Drafting of the manuscript: Annweiler, Abraham, Beauchet, Calès, and Redureau. Critical revision of the manuscript for important intellectual content: Fantino and De Decker. Statistical expertise: Annweiler. Administrative, technical, or material support: Beauchet. Study supervision: Annweiler.

Sponsor's Role: None.

REFERENCES

1. Melamed ML, Muntner P, Michos ED et al. Serum 25-hydroxyvitamin D levels and the prevalence of peripheral arterial disease: Results from NHANES 2001 to 2004. Arterioscler Thromb Vasc Biol 2008;28: 1179–1185.
2. Barnard K, Colon-Emeric C. Extraskeletal effects of vitamin D in older adults: Cardiovascular disease, mortality, mood, and cognition. Am J Geriatr Pharmacother 2010;8:4–33.
3. Freedman BI, Wagenknecht LE, Hairston KG et al. Vitamin D, adiposity, and calcified atherosclerotic plaque in African-Americans. J Clin Endocrinol Metab 2010;95:1076–1083.
4. Razzaque MS. The dualistic role of vitamin D in vascular calcifications. Kidney Int 2011;79:708–714.
5. Norgren L, Hiatt WR, Dormandy JA et al. Inter-Society Consensus for the management of peripheral arterial disease (TASC II). J Vasc Surg 2007;45: S5–S67.
6. Allison MA, Hiatt WR, Hirsch AT et al. A high ankle-brachial index is associated with increased cardiovascular disease morbidity and lower quality of life. J Am Coll Cardiol 2008;51:1292–1298.
7. Bischoff-Ferrari HA, Giovannucci E, Willett WC et al. Estimation of optimal serum concentrations of 25-hydroxyvitamin D for multiple health outcomes. Am J Clin Nutr 2006;84:18–28.
8. Bas A, Lopez I, Perez J et al. Reversibility of calcitriol-induced medial artery calcification in rats with intact renal function. J Bone Miner Res 2006;21:484–490.
9. Zebger-Gong H, Müller D, Diercke M et al. 1,25-Dihydroxyvitamin D3-induced aortic calcifications in experimental uremia: Up-regulation of osteoblast markers, calcium-transporting proteins and osterix. J Hypertens 2011;29:339–348.
10. Bolland MJ, Avenell A, Baron JA et al. Effect of calcium supplements on risk of myocardial infarction and cardiovascular events: Meta-analysis. BMJ 2010;341:c3691. doi: 10.1136/bmj.c3691.

PULMONARY FEATURES ASSOCIATED WITH BEING UNDERWEIGHT IN OLDER MEN

To the Editor: Body mass index (BMI) is one of the most potent prognostic markers in chronic obstructive pulmonary disease (COPD),[1] but it is unclear whether low body weight worsens the symptoms, respiratory function, and prognosis of COPD or only reflects one aspect of advanced COPD.

It is difficult for people with COPD to differentiate the effects of being underweight on pulmonary symptoms and function from the worsening of COPD itself, because a cachexic state is frequently associated with the advance of COPD. One effective approach to this uncertainty would be to assess the respiratory function and symptoms of people with severely low body weight due to causes not associated with respiratory function.[2] These observations would indicate whether nutritional therapy could mitigate respiratory symptoms and dysfunction in people with COPD.

This report presents a case of an 85-year-old man who underwent total gastrectomy and cholecystectomy because of stomach cancer. He had never smoked and had shown no shortness of breath during exercise. He had mild anemia and was diagnosed with stomach cancer. No major postoperative complications occurred, and he left the hospital 12 days after the surgery, but he had severe loss of appetite and his BMI decreased from 25.0 kg/m^2 before the surgery to 17.2 kg/m^2 5 months after the surgery. Although no pulmonary complications were detected on chest computed tomography, he complained of shortness of breath during light exercise corresponding to Medical Research Council (MRC) dyspnea scale Grade 4. His vital capacity (VC) decreased from 3.04 L before surgery to 1.96 L after, and his forced expiratory volume in 1 second (FEV_1)/VC ratio paradoxically increased from 62.8% to 93.9%, masking the preexisting mild obstructive pulmonary disorder. His residual volume to total lung capacity (RV/TLC) ratio reached 62.6% after the surgery, whereas TLC was 94.0% of the predicted value. No hypoxia was observed despite the severe shortness of breath.

The pulmonary features of older outpatients with severely low body weight without respiratory diseases were

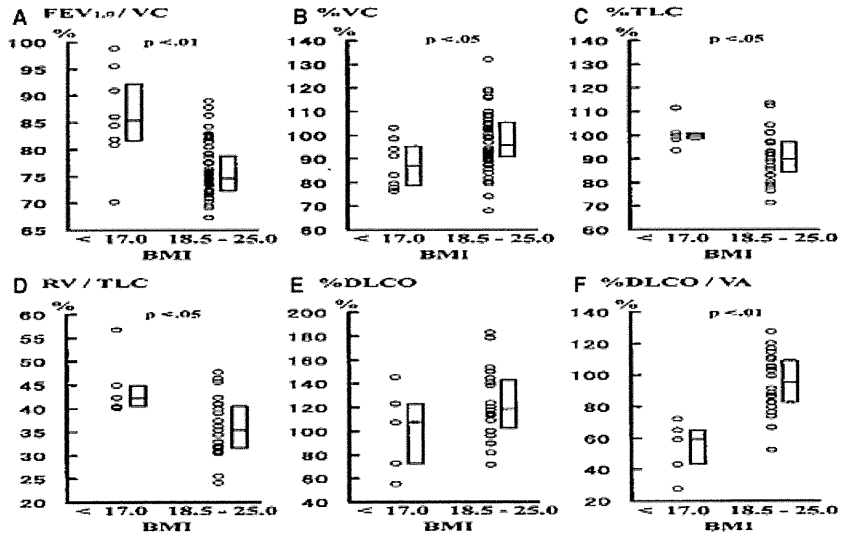

Figure 1. Pulmonary function of underweight patients and normal-weight patients. Ratio of forced expiratory volume in 1 second to VC (FEV_1/VC), percentage of VC (%VC), percentage of TLC (%TLC), residual volume to total lung capacity (RV/TLC) ratio, percentage of diffusing capacity of carbon monoxide (%DLCO), and %DLCO to alveolar volume (%DLCO/VA) of older men with a body mass index (BMI) less than 17.0 kg/m^2 were compared with those of older men with a BMI of 18.5 to 25.0 kg/m^2. Each circular point indicates measured individual data. The boxes indicate the 25th percentile, median, and 75th percentile values. The FEV_1/VC ratio, %TLC, and the RV/TLC ratio were significantly higher, and %VC and %DLCO/VA were significantly lower in the men with BMI < 17.0 kg/m^2.

also investigated. The study population included men aged 65 and older who visited the Department of Geriatric Medicine at the University of Tokyo Hospital from September to October 2008 and men aged 65 and older who visited the Department of Respiratory Medicine at the University of Tokyo Hospital in October 2009. Spirometry had been performed according to Japanese Respiratory Society guidelines.[3] The ethics committee in the medical department at the University of Tokyo approved this study protocol.

The study excluded patients with a FEV_1/FVC ratio of less than 70% or other pulmonary complications observable on chest radiographs or documented in medical records, such as pulmonary malignancies, marked sequelae of pulmonary tuberculosis, interstitial pneumonia, massive pleural effusion, active pneumonia, acute or refractory heart failure, history of lobectomy, and bronchial asthma. Angina pectoris, palpitation, and paroxysmal dyspnea were excluded from the evaluations of respiratory symptoms.

Respiratory symptom and function data were obtained from eight older men with a BMI less than 17.0 kg/m^2. The cause of low body weight of these men were depression (n = 2), a past history of partial or total gastrectomy (n = 3), a past history of ulcerative colitis (n = 1), and no specific diseases (n = 2). Five had shortness of breath when walking up a slight hill, and two complained of shortness of breath even during light exercise, corresponding to MRC dyspnea scale Grades 3 to 4, as observed in the presented case. None had signs of hypoxia at rest.

Data were also obtained from 50 older men with a BMI between 18.5 and 25.0 kg/m^2 (normal weight) without evident pulmonary disease. Only four had shortness of breath during exercise ($P = .001$, Fisher exact test), and none had severe shortness of breath corresponding to MRC dyspnea scale Grade 3 or greater.

The pulmonary function data of the older underweight men without pulmonary diseases (BMI < 17.0 kg/m^2) were compared with those of the older normal-weight men without pulmonary diseases (BMI 18.5–25.0 kg/m^2) using the Mann-Whitney *U* test. DLCO/VA is the ratio of diffusing capacity of carbon monoxide to alveolar volume. Percentage of VC (%VC), percentage of TLC (%TLC), and the percentage of DLCO/VA (%DLCO/VA) were determined by calculating the percentage of individual data to the predicted values; %TLC ($P = .04$) and RV/TLC ratios ($P = .02$) were significantly higher in the underweight men than in those who were normal weight (Figure 1). The %VC and %DLCO/VA was significantly lower in the underweight men than in those who were normal weight (%VC, $P = .04$; %DLCO/VA, $P = .001$; Figure 1). The FEV_1/VC ratio was paradoxically greater in the underweight men, maybe because of the lower VC and higher RV/TLC ratios ($P = .003$).

Being severely underweight involves weakened muscular strength. The higher RV/TLC ratios, lower VC, and higher FEV_1/VC ratios of the older underweight men could be due to the weakened respiratory muscles, especially expiratory muscles.[4] Higher %TLC and lower %DLCO/VA without a concomitant DLCO decrease would indicate lung hyperinflation in the older underweight men. These findings are also consistent with reported lung pathology in starved animals, which shows endogenous alveolar loss without necrosis or inflammation.[5]

These findings support the clinical benefit of promoting nutritional therapy to avoid excessive weight loss in people with COPD and older adults.[6] Further prospective studies evaluating the changes in respiratory symptoms and

function associated with low body weight or alterations in body composition are warranted.

Yasuhiro Yamaguchi, MD
Shinicihiro Hibi, MD
Masaki Ishii, MD
Yoko Hanaoka, MD
Department of Geriatric Medicine

Hidenori Kage, MD
Department of Respiratory Medicine

Hiroshi Yamamoto, MD
Department of Geriatric Medicine
Yasuhiro Yamauchi, MD
Department of Respiratory Medicine

Masato Eto, MD
Department of Geriatric Medicine

Takahide Nagase, MD
Department of Respiratory Medicine

Yasuyoshi Ouchi, MD
Department of Geriatric Medicine
Graduate School of Medicine
University of Tokyo
Tokyo, Japan

ACKNOWLEDGMENTS

This work was supported by grants-in-aid for young scientists from the Ministry of Education, Science, Sports and Culture of Japan.

Conflict of Interest: No conflicts of interest to disclose.

Author Contributions: Yasuhiro Yamaguchi: coordinator of study concept and design, data analysis, preparation of manuscript. Shinnicihiro Hibi: acquisition of data. Masaki Ishii and Yoko Hanaoka: data analysis. Hidenori Kage: data analysis and preparation of manuscript. Hiroshi Yamamoto: interpretation of data. Yasuhiro Yamauchi: acquisition of data and subjects. Masato Eto: interpretation of data. Takahide Nagase: coordinator of study concept and design. Yasuyoshi Ouchi: coordinator of study concept and design.

Sponsor's Role: None.

REFERENCES

1. Celli BR, Cote CG, Marin JM et al. The body-mass index, airflow obstruction, dyspnea, and exercise capacity index in chronic obstructive pulmonary disease. N Engl J Med 2004;350:1005–1012.
2. Gardini Gardenghi G, Boni E, Todisco P et al. Respiratory function in patients with stable anorexia nervosa. Chest 2009;136:1356–1363.
3. Tamura G, Aizawa H, Nagai A et al. Common prediction equations of respiratory function tests from children to adults in Japan. Nihon Kokyuki Gakkai Zasshi 2007;45:526–542.
4. Kreitzer SM, Saunders NA, Tyler HR et al. Respiratory muscle function in amyotrophic lateral sclerosis. Am Rev Respir Dis 1978;117:437–447.
5. Massaro D, Massaro GD, Baras A et al. Calorierelated rapid onset of alveolar loss, regeneration, and changes in mouse lung gene expression. Am J Physiol 2004;286:L896–L906.
6. Feldblum I, German L, Castel H et al. Individualized nutritional intervention during and after hospitalization: The Nutrition Intervention Study clinical trial. J Am Geriatr Soc 2011;59:10–17.

LIVING WITH STAIRS: FUNCTIONING IN A LARGE COHORT OF OLDER AUSTRALIAN ADULTS

To the Editor: Stair climbing has been encouraged as a health promotion measure in the general population,[1] and health benefits have been demonstrated in young people,[2] but these benefits may not extend to older adults, and living in a building with stairs may prove challenging for older adults. The difficulty that older adults experience in climbing up or down stairs has been associated with a number of chronic conditions, including hypertension, arthritis, and depression.[3] Living with stairs may increase the risk of fall-related injury or death. Nonfatal injuries on stairs are common in older persons and are more likely to result in hospitalization than accidents in younger people; 10% of fall-related deaths occur as a consequence of falls on stairs.[4] For older adults with no partner, managing stairs could be problematic, because many receive support in activities of daily living from their spouses.[5] This is potentially more germane for women, who tend to outlive their spouses. This study aimed to examine health-related difficulties with stairs in a large, prospective cohort study of older adults. The hypothesis was that older adults with a chronic condition and without a partner would report greater difficulty in managing stairs.

METHODS

Data were obtained from the Men, Women and Ageing (MWA) project, which incorporates data from two population-based longitudinal studies that began in 1996: the 1921 to 1926 birth cohort of the Australian Longitudinal Study on Women's Health (ALSWH) and the Perth Health in Men Study (HIMS). Detailed methods for both studies have been described elsewhere.[6,7] The human research ethics committees of the University of Newcastle and the University of Queensland approved the research protocol for the ALSWH. The ethics committee of the University of Western Australia approved the HIMS research protocol.

This analysis is based on data drawn from the fifth ALSWH survey and the third HIMS survey, both conducted in 2008. Participants in HIMS live in an urban area (Perth, Western Australia), whereas ALSWH participants are a national sample including rural and regional areas. To eliminate potential confounding related to area of residence, analyses for this study used data from ALSWH urban residents only. At the time of the 2008 surveys, the women were aged 82 to 87, and the men were aged 77 to 91. For this analysis, the age range of 82 to 87 was used for women (n = 2,421) and men (n = 1,072).

Measures

Difficulty in managing stairs was measured according to a question drawn from the Medical Outcomes Study 36-item Short Form,[8] which asks "Does your health now limit you in these activities? If so, how much: climbing several flights of stairs; climbing one flight of stairs." Responses were yes, limited a lot; yes, limited a little; or no, not limited at all.

Participants reported whether they had ever been diagnosed with any of the following chronic medical conditions: arthritis, osteoporosis, chronic obstructory pulmo-

The American Journal of Pathology, Vol. 180, No. 2, February 2012

DOI: 10.1016/j.ajpath.2011.10.031

Musculoskeletal Pathology

Antibodies against Muscle-Specific Kinase Impair Both Presynaptic and Postsynaptic Functions in a Murine Model of Myasthenia Gravis

Shuuichi Mori,* Sachiho Kubo,*
Takuyu Akiyoshi,*† Shigeru Yamada,*
Tsuyoshi Miyazaki,* Harumi Hotta,‡
Junzo Desaki,§ Masahiko Kishi,¶ Tetsuro Konishi,‖
Yuri Nishino,**††‡‡ Atsuo Miyazawa,**††‡‡
Naoki Maruyama,§§ and Kazuhiro Shigemoto*

From the Departments of Geriatric Medicine, Autonomic Nervous System,‡ and Molecular Regulation of Aging,§§ Tokyo Metropolitan Institute of Gerontology, Tokyo; the Department of Geriatric Medicine,† Graduate School of Medicine and Faculty of Medicine, the University of Tokyo, Tokyo; the Department of Integrated Basic Medicine Research,§ Ehime University School of Medicine, Ehime; the Department of Internal Medicine,¶ Toho University Sakura Medical Center, Chiba; the Department of Neurology,‖ National Hospital Organization Utano National Hospital, Kyoto; the Bio-Multisome Research Team,** RIKEN SPring-8 Center, Harima Institute, Hyogo; the Graduate School of Life Science,†† University of Hyogo, Hyogo; and Core Research for Evolutional Science and Technology,‡‡ Japan Science and Technology Agency (CREST-JST), Tokyo, Japan*

Antibodies against acetylcholine receptors (AChRs) cause pathogenicity in myasthenia gravis (MG) patients through complement pathway-mediated destruction of postsynaptic membranes at neuromuscular junctions (NMJs). However, antibodies against muscle-specific kinase (MuSK), which constitute a major subclass of antibodies found in MG patients, do not activate the complement pathway. To investigate the pathophysiology of MuSK-MG and establish an experimental autoimmune MG (EAMG) model, we injected MuSK protein into mice deficient in complement component five (C5). MuSK-injected mice simultaneously developed severe muscle weakness, accompanied by an electromyographic pattern such as is typically observed in MG patients. In addition, we observed morphological and functional defects in the NMJs of EAMG mice, demonstrating that complement activation is not necessary for the onset of MuSK-MG. Furthermore, MuSK-injected mice exhibited acetylcholinesterase (AChE) inhibitor-evoked cholinergic hypersensitivity, as is observed in MuSK-MG patients, and a decrease in both AChE and the AChE-anchoring protein collagen Q at postsynaptic membranes. These findings suggest that MuSK is indispensable for the maintenance of NMJ structure and function, and that disruption of MuSK activity by autoantibodies causes MG. This mouse model of EAMG could be used to develop appropriate medications for the treatment of MuSK-MG in humans. ***(Am J Pathol 2012, 180:798–810; DOI: 10.1016/j.ajpath.2011.10.031)***

Myasthenia gravis (MG), the most common disorder of neuromuscular synapses, is caused by autoantibodies against postsynaptic membranes at neuromuscular junctions (NMJs).[1,2] The characteristic clinical features of this autoimmune disease include ptosis, fatigue, and muscular weakness. In 2001, autoantibodies against muscle-specific kinase (MuSK) were found in 70% of patients with generalized MG who lacked antibodies to acetylcholine receptors (AChRs).[3] MuSK, a receptor tyrosine kinase, is concentrated at NMJs from the earliest stages of synaptogenesis and is required for the formation of NMJs during development.[4] Recent studies demonstrated that MuSK is activated by dimerization with low-density lipo-

Supported by grants from the Health Science Research Grants for Research on Psychiatric and Neurological Diseases and Mental Health (H19-Psycho-General-19 to K.S.), Comprehensive Research of Aging and Health (H22-Aging-General-002 to K.S.) from the Ministry of Health, Labor, and Welfare, Japan, Grants-in-Aid for Scientific Research on Innovative Area (21200023 to K.S.), Grants-in-Aid for Scientific Research (C) (21591102 to K.S.), Grants-in-Aid for Young Scientists (B) (23791009 to S.M.) from the Ministry of Education, Science, and Culture, Japan, and Intramural Research Grant (22-5 to K.S.) for Neurological and Psychiatric Disorders of National Center of Neurology and Psychiatry.

Accepted for publication October 25, 2011.

Supplemental material for this article can be found at *http://ajp.amjpathol.org* or at doi: 10.1016/j.ajpath.2011.10.031.

Address reprint requests to Kazuhiro Shigemoto, M.D., Ph.D., Tokyo Metropolitan Institute of Gerontology, Department of Geriatric Medicine, Sakaecho 35-2, Itabashi-ku, Tokyo 173-0015 Japan. E-mail: kazshige@tmig.or.jp.

protein receptor-related protein 4 (LRP4) on agrin binding to LRP4.[5,6]

We previously developed a model of experimental autoimmune myasthenia gravis (EAMG) caused by MuSK antibodies (MuSK Abs) by active immunization of rabbits with recombinant soluble MuSK protein.[7] In addition, passive transfer of human MuSK Abs from MG patients into mice was shown to cause MG.[8] These studies not only demonstrate the pathogenicity of MuSK Abs in the onset of MG, but also suggest that MuSK is required for the maintenance of mature NMJs.

Although previous studies have suggested that the disruption of NMJ maintenance by MuSK Abs might cause MG, several questions remain regarding the pathology of MuSK-MG. First, MuSK Abs in MG patients are mainly composed of the IgG4 subclass.[9,10] IgG4 antibodies do not activate the classical complement pathway, and thus cannot act through the same mechanism observed for AChR antibodies in MG.[2] Additionally, several studies have shown that small amounts of additional complement-fixing subclasses of MuSK and AChR Abs are also detectable in MuSK-MG patients,[9–11] casting doubt on the pathogenicity of MuSK Abs. Therefore, it is essential to determine whether MuSK Abs cause MG without complement activation.

Second, a number of clinical studies have shown that MuSK-MG constitutes a distinct subclass of MG. For example, patients with MuSK-MG are more prone to severe muscle weakness with respiratory crises and eventual atrophy than those with AChR-MG,[12,13] and thus require emergent and aggressive therapies. In addition, although acetylcholinesterase (AChE) inhibitors are often used effectively as symptomatic treatment for AChR-MG,[1,2] MuSK-MG patients frequently either are unresponsive to this treatment or develop cholinergic crises characterized by increasing muscle weakness.[14] A thorough understanding of the unique pathophysiology of MuSK-MG is crucial for the development and assessment of appropriate medications in the future.

To resolve this critical issue, we generated a new animal model in which 100% of mice synchronously develop EAMG after immunization with MuSK protein. This model not only reveals the pathogenic mechanisms involved in MuSK-MG, but also clarifies the role of MuSK at mature NMJs.

Materials and Methods

Preparation of Recombinant MuSK Protein

The fusion protein expression construct, consisting of the rat MuSK ectodomain and a 3′ myc/His-tag sequence, was generated as described previously.[7] 293-F cells were transfected with FreeStyle MAX reagent (Invitrogen) according to the manufacturer's instructions. Secreted recombinant MuSK protein was purified using Ni-Sepharose (GE Healthcare, Piscataway, NJ), pooled, and concentrated. The purity of the recombinant protein was determined by SDS-PAGE with Coomassie blue staining, and the concentration was determined using a Quant-iT assay kit (Invitrogen) with bovine serum albumin as a standard.

Immunization of Mice

All animal procedures used were approved by the Animal Care and Use Committee of Tokyo Metropolitan Geriatric Hospital and Institute of Gerontology. A/WySnJ and C3-deficient mice were obtained from the Jackson Laboratory (Bar Harbor, ME). A/J, B10.A-*H2*^{a}, BALB/c, and C57BL/6 mice were obtained from Japan SLC (Hamamatsu, Japan). DBA/2 and FVB/N mice were obtained from CLEA Japan (Fuji, Japan). All mice were used after 8 weeks of age. On day 0, adult female mice were anesthetized with tribromoethanol and injected subcutaneously in the hind footpads with 20 μg MuSK emulsified with complete Freund's adjuvant. All mice were boosted with 20 μg MuSK emulsified with incomplete Freund's adjuvant on day 14. All C57BL/6J and C3-deficient mice received a third injection of the same dose emulsified with incomplete adjuvant on day 28. Control mice were injected with equal volumes of PBS or equal doses of ovalbumin (OVA) emulsified with adjuvant in the same manner and on the same schedule. For comparison with MuSK-injected mice, A/WySnJ mice were injected with 20 μg AChR protein, which was purified from *Torpedo californica* as described previously[15] and emulsified with adjuvant on days 0, 14, and 42. When antigen-immunized mice exhibited a prominent cervical hump and gait disturbance, they were analyzed for EAMG.

Measurement of Muscle Strength

Forelimb muscle strength was determined by using an MK-380M grip strength meter (Muromachi Kikai, Tokyo, Japan). Mice were allowed to grip the cage lid while being held by the tail, with hindlimbs suspended, and were pulled horizontally until the grip was released. Seven measurements were performed per mouse. The highest and lowest values were discarded, and the average of the five remaining measurements was used for statistical evaluation.

Measurements of Titer and Subclasses of MuSK Antibodies

Wells of ELISA plates were coated with purified rat MuSK (150 ng/well) diluted in Tris-buffered saline. After a washing with 0.1% Tween-20/Tris-buffered saline, plates were blocked with 4% BlockAce (Dainippon Pharmaceutical, Osaka, Japan), then incubated for 3 hours at 37°C with diluted sera (1:1000 in Tris-buffered saline) from MuSK-immunized and preimmune mice. The plates were washed and then incubated for 1 hour at 37°C with HRP-conjugated antibodies against anti-mouse IgG (1:3000 in 0.1% Tween-20/Tris-buffered saline; GE Healthcare), followed by another washing and reaction with a 3,3′,5,5′-tetramethylbenzidine liquid substrate system (Sigma-Aldrich, St. Louis, MO). The colorimetric reaction was stopped by 2 mol/L HCl (2N HCl), and the values of

absorbance at 450 nm were determined as titers of MuSK antibodies. Subclasses of MuSK antibodies were determined using a Mouse Typer sub-isotyping kit (Bio-Rad Laboratories, Hercules, CA) according to the manufacturer's instructions. Only the measurement of IgE was performed by using antibody (Nordic Immunological Laboratories, Eindhoven, The Netherlands) not in the kit. In isotyping analysis, sera from MuSK-immunized mice were diluted 1:3000.

Electromyography

Changes in compound muscle action potential (CMAP) were studied using a PowerLab 4/26 data acquisition system (ADInstruments, Colorado Springs, CO). Mice were anesthetized with tribromoethanol and maintained at 37°C on a thermoregulation device. Paired stimulating electrodes separated by 2 to 3 mm were inserted intramuscularly near the sciatic notch for supramaximal stimulation at 3 Hz. Recording electrodes were inserted in the medial compartment of the gastrocnemius muscle and near the insertion of the Achilles tendon. To isolate stimulus artifacts, a ground electrode was placed between the stimulus and recording electrodes. Decrement was calculated as percent amplitude change between the first and least CMAPs evoked by a train of 10 impulses. If the amplitude of the first CMAP was the least within the measurement, the decrement was designated as 0%. In drug treatment experiments, neostigmine bromide (37.5 μg/kg; Sigma-Aldrich) was given by intraperitoneal injection. A typical mouse weighing 20 g received 100 μL of freshly prepared solution containing 7.5 μg/mL of neostigmine bromide in PBS. After 20 minutes, the effect of drug treatment was evaluated via electromyography (EMG).

In Vitro *Electrophysiology*

Left phrenic nerve and hemi-diaphragm muscle preparations were made after tribromoethanol anesthetization. The muscle specimen was placed in a 1.0-mL chamber filled with Tyrode's solution, which was constantly oxygenized by a gas mixture of 95% O_2/5% CO_2 released close to the fluid surface. Membrane potentials and miniature endplate potentials (MEPPs) were recorded at room temperature (18°C to 22°C) using a glass microelectrode filled with 3 mol/L KCl via a PowerLab 4/26 data acquisition system. To measure evoked endplate potentials (EPPs), μ-conotoxin GIIIB (Peptide Institute, Osaka, Japan) was added to the chamber (1 μmol/L final concentration) to suppress muscle contraction, and the phrenic nerve was stimulated by silver electrodes with supramaximal voltage at 0.7 Hz. Amplitudes of EPPs and MEPPs were standardized to a membrane potential of −75 mV. Quantal content was calculated by applying the values of mean MEPP amplitude, mean EPP amplitude, and membrane potential in the same muscle fiber to a formula reported previously.[16,17] To analyze rate of EPP decay, an exponential function was fitted to the falling phase portion from 80% to 20% of EPP peak value, and the decay time constant (τ) was calculated using the Peak Parameter program in the LabChart software package (version 7.1.2; ADInstruments). The MEPP frequency was calculated from a >1 minute recording in each NMJ. To exclude the effects of μ-conotoxin treatment and nerve stimulation on spontaneous neurotransmission, frequency measurements were performed separately from those of quantal content. Data for ≥10 NMJs were obtained from each normal or MuSK-immunized mouse.

Whole-Mount Staining of NMJs

For quantification of nerve terminals and AChR and AChE staining areas, whole-mount staining of soleus muscles was performed. Soleus muscles were removed and fixed in 1% paraformaldehyde/PBS for 10 minutes at room temperature, rinsed in PBS, and incubated with 0.1 mol/L glycine/PBS. After filleting muscles into several sheets of fibers using microdissection scissors, muscle slices were incubated with either rhodamine or Alexa Fluor 647-conjugated α-bungarotoxin (BTx, 40 nmol/L in PBS; Invitrogen) to label AChRs for 1 hour at room temperature. Muscles were then rinsed in PBS, permeabilized in methanol at −20°C, washed again in PBS for 30 minutes, and blocked for 1 hour in 2% bovine serum albumin/0.3% TritonX-100/PBS. Slices were then incubated overnight at 4°C in a cocktail of primary antibodies diluted in blocking solution. Axons and nerve terminals were labeled with rabbit polyclonal antibodies against neurofilament (1:400; Millipore-Chemicon International, Temecula, CA) and synaptophysin (1:100; Invitrogen).

For quantification of nerve terminals, muscles were incubated only with anti-synaptophysin. Rabbit polyclonal antibody against AChE (1:1000) was generated by Dr. Terrone L. Rosenberry (Mayo Clinic College of Medicine). Antiserum against collagen Q (ColQ, 1:2000) was prepared by injecting Wistar rats with a synthetic peptide corresponding to residues 35 to 51 of the ColQ deduced primary sequence coupled to keyhole limpet hemocyanin. After incubation with primary antibodies, muscles were rinsed three times (20 minutes each) in PBS and incubated overnight at 4°C with either Alexa Fluor 488- or Alexa Fluor 555-conjugated secondary antibodies (1 μg/mL in blocking solution; Invitrogen) corresponding to the hosts of the primary antibodies. After incubation with secondary antibodies, muscles were rinsed three times (20 minutes each) in PBS and flat-mounted in a SlowFade antifade kit (Invitrogen) for confocal microscopic analysis. For quantification of AChR staining intensity, diaphragms were dissected and fixed in 1% paraformaldehyde/PBS for 1 hour at room temperature, rinsed in PBS, and incubated with 0.1 mol/L glycine/PBS. Some pieces of left hemi-diaphragm were incubated overnight at 4°C with Alexa Fluor 488-BTx (40 nmol/L in PBS; Invitrogen). Muscles were then rinsed three times (20 minutes each) in PBS and flat-mounted in the same way as soleus muscles. Confocal images were acquired with a Leica TCS SP5 confocal laser scanning unit, using a 63× glycerin objective on a Leica DMI6000 microscope (Leica Microsystems, Wetzlar, Germany), and images of ≥30 NMJs were acquired from each control or MuSK-immunized

mouse (n = 3 mice/group). For quantification of synaptophysin, AChR and AChE staining areas were quantified on a maximum projection of confocal images with ImageJ software (version 1.42q; NIH, Bethesda, MD). The ImageJ Analyze Particle program was used to quantify the areas of each staining experiment.

Electron Microscopy

After tribromoethanol anesthetization, tibialis anterior muscles were exposed and fixed *in situ* with 4% glutaraldehyde/0.1 mol/L phosphate buffer at pH 7.3 for 5 minutes. Muscles were then dissected, cut into small strips, postfixed with the same solution for 2 hours at room temperature, rinsed several times in distilled water, and further postfixed with 1% unbuffered osmium tetroxide for 30 minutes. For SEM observation, muscles were treated with a HCl-hydrolysis procedure to remove intramuscular connective tissues as described previously.[18] After a drying via the critical point method and then a sputter coating with platinum, specimens were examined in a Hitachi S-800 SEM (Hitachi High-Technologies, Tokyo, Japan). For TEM observation, diaphragms were fixed *in situ* by injecting the fixative intrathoracically and intraperitoneally until these cavities were filled. Small pieces of fixed muscle were block-stained with 3% aqueous uranyl acetate for 2 hours and embedded in Epon 812 resin (Nissin EM, Tokyo, Japan) after dehydration through an ethanol series. Ultrathin sections were cut with an Ultracut E ultramicrotome (Reichert-Jung, Austria), doubly stained with uranyl acetate and lead citrate, and then examined with a Hitachi HU-12A transmission microscope (Hitachi High-Technologies). For morphometric analysis, TEM images were scanned and the density of junctional folds was determined by the number of folds divided by the length of the presynaptic membrane using ImageJ software (version 1.42q). Images of ≥10 NMJs from each mouse were obtained for quantification.

Preparation of IgG Fractions and Fab Fragments from MuSK Antisera

Sera from MG-affected mice were collected, and the IgG fraction was purified with Protein G-Sepharose (GE Healthcare) as anti-MuSK IgG. Fab fragments of anti-MuSK IgG were prepared using a Pierce mouse IgG1 Fab preparation kit (Thermo Scientific, Rockford, IL) with papain digestion. As a control, IgG fractions (normal IgG) and Fab fragments (normal Fab) were prepared from sera of preimmune mice using the same method.

AChR Clustering Assay

The C2C12 cell line was obtained from the American Type Culture Collection (ATCC, Manassas, VA) and used for three to eight passages. Cells were cultured in 12-well plates as myoblasts in 10% fetal calf serum (FCS)/Dulbecco's modified Eagle's medium. When the cells reached confluency, myotube formation was induced by replacing the medium with 2% horse serum/Dulbecco's modified Eagle's medium. The cells were incubated for 3 days, with fresh medium exchange every day, until full differentiation into multinucleated myotubes was observed morphologically. Preparation of recombinant agrin protein was as described previously.[7] Myotubes were treated with 10 μg/mL anti-MuSK IgG or Fab for 30 minutes, and then incubated for 16 hours with 1 nmol/L agrin. AChR clustering was visualized after incubation with 40 nmol/L Alexa Fluor 594-BTx (Invitrogen) in fusion medium for 1 hour at 37°C before fixation. Fluorescence images of myotubes were acquired using a 20× objective on a Leica DMI6000 microscope; the number of AChR clusters in six randomly selected fields was counted.

MuSK Phosphorylation Assay

The C2C12 myotubes were treated with either 10 μg/mL anti-MuSK IgG or Fab. After 30 minutes, half of the myotube cultures were further treated for 30 minutes with 1 nmol/L agrin, and the remaining cultures were left untreated. The myotubes were lysed and solubilized using a protease inhibitor cocktail (complete EDTA-free; Roche Applied Science, Indianapolis, IN) with 2 mmol/L sodium orthovanadate. Extracts were immunoprecipitated with antibodies directed against MuSK, and the resulting precipitates were immunoblotted with either a mixture of the anti-phosphotyrosine antibodies 4G10 (Millipore, Billerica, MA) and PY20 (Millipore-Chemicon International) or MuSK antibodies. Antibodies directed against MuSK were generated in rabbits as described previously.[7] Band intensities of immunoblots were assessed using ImageJ software (version 1.42q).

Statistical Analysis

Significant differences between control and MuSK-injected mice were analyzed by unpaired t-test. Paired t-test was used to analyze the effect of neostigmine treatment in EMG experiments. Analysis of variance was used to assess AChR clustering and MuSK phosphorylation assays. P values of <0.05 were considered statistically significant.

Results

MuSK Protein Injection Results in Synchronous Muscle Weakness with Weight Loss

A/WySnJ mice were injected with 20 μg of MuSK protein on days 0 and 14 of the experiment. Because A/WySnJ mice carry mutations that result in C5 deficiency,[19] these mice cannot generate a lytic membrane attack complex and are therefore highly resistant to EAMG after AChR immunization.[20,21] All mice (n = 18) injected with MuSK manifested severe muscle weakness with tremors within 2 weeks of the second injection. These symptoms occurred synchronously in all animals, along with the appearance of a prominent cervicothoracic hump, indicat-

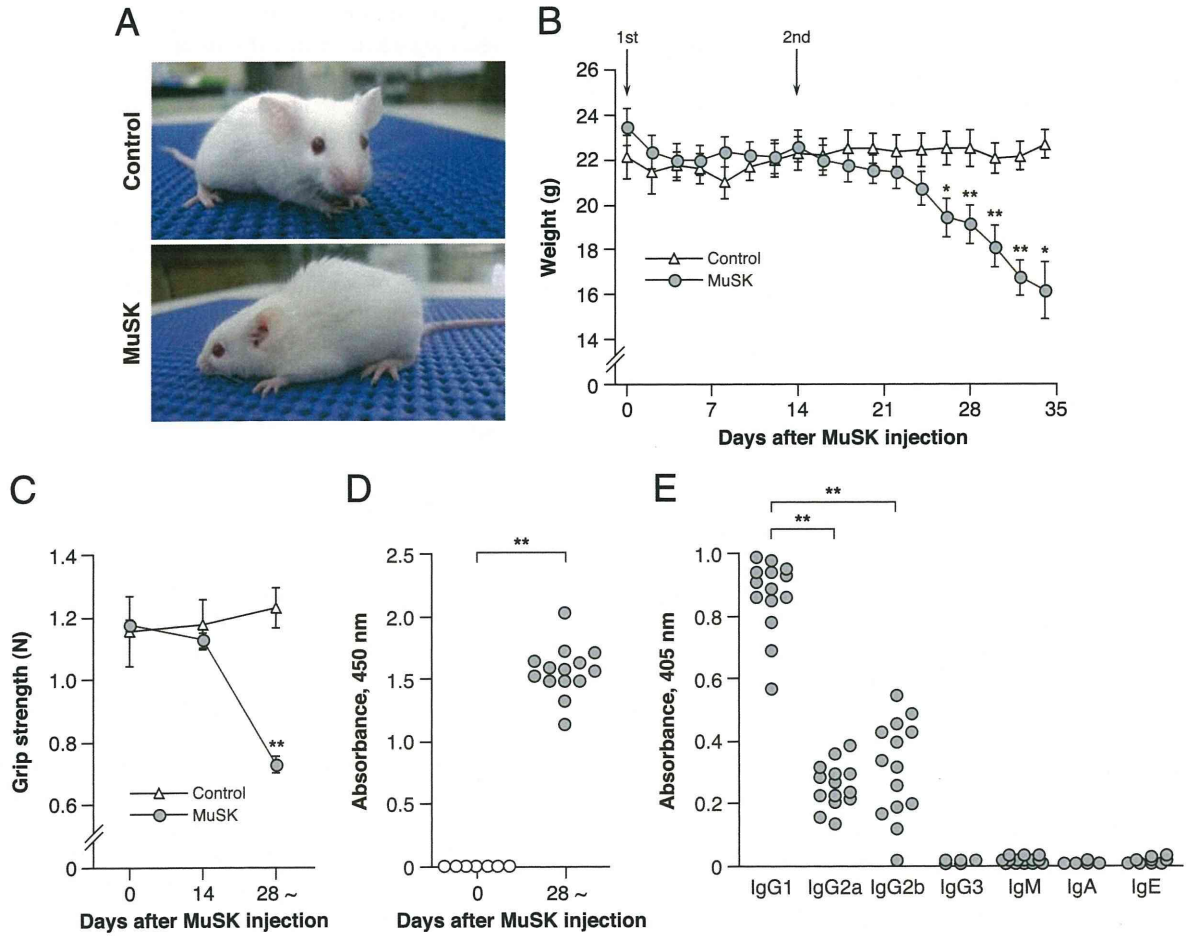

Figure 1. Manifestation of MG-like phenotypes after MuSK injection of A/WySnJ mice. **A:** A/WySnJ mice injected with MuSK protein exhibited a prominent cervical hump and were unable to raise their heads. Control mice injected with vehicle showed no such malformation. MuSK-injected mice lost weight (**B**) and muscle strength (**C**) after the second injection, compared with control mice. Significant weight reduction was observed in MuSK-injected mice at day 26 after the first injection. $n = 5$, control; $n = 18$, MuSK-injected. Data are reported as means ± SEM. $^{*}P < 0.05$; $^{**}P < 0.01$ versus control A/WySnJ mice (*t*-test). **D:** Change in MuSK immunoreactivities of sera after MuSK immunization. Sera from MG-affected mice contained a high titer of MuSK Abs. Sera were prediluted 1:1000 for assay. Values of absorbance at 450 nm were determined as MuSK immunoreactivity. $^{**}P < 0.01$ versus preimmune sera (*t*-test). **E:** Isotyping analysis of MuSK Abs. MuSK Abs were predominantly of the IgG1 subclass, with small amounts of IgG2a and IgG2b, but no detectable IgG3, IgM, IgA, or IgE. Sera were prediluted 1:3000 for assay. Values of absorbance at 405 nm were determined as amounts of MuSK Ab subclasses. $^{**}P < 0.01$ versus IgG1 subclass (analysis of variance). Open symbols, control; filled symbols, MuSK.

ing weak cervical extensor muscles (Figure 1A). In addition, MuSK-injected mice exhibited significant weight loss and muscle weakness (Figure 1, B and C). By contrast, neither vehicle-injected mice ($n = 5$; Figure 1, B and C) nor OVA-injected mice ($n = 5$; data not shown) exhibited weight loss or muscle weakness. We also injected three A/WySnJ mice with *Torpedo californica* AChR protein three times (at days 0, 14, and 42) and found no effect on body weight or muscle strength in these mice (data not shown).

IgG1 Is a Predominant Subclass in MuSK Abs

To test whether muscle weakness of the mice correlates with serum titers of MuSK protein, we used ELISA. Anti-MuSK IgG antibodies were detectable in all MuSK-injected mice, whereas control mice ($n = 5$) had no detectable antibodies to MuSK, which was similar to the preimmune sera (Figure 1D). Isotyping analysis revealed that MuSK Abs were predominantly of the IgG1 subclass, along with smaller amounts of IgG2a and IgG2b (Figure 1E). No other subclasses tested were detected in the MuSK Abs. Mouse IgG1 has functional similarities with human IgG4 in terms of electrophoretic mobility and T-helper type 2 dependency for production.[22] Thus, MuSK-MG in patients and in A/WySnJ mice seems to share a common immune regulatory pathway.

MuSK Abs Change Both Presynaptic and Postsynaptic Structures

To assess directly whether the presence of MuSK Abs results in NMJ structural changes, whole mounts of soleus muscles from MuSK-injected and control mice were double-labeled with BTx (a probe for AChRs), as well as a cocktail of antibodies against neurofilaments and the synaptic vesicle marker synaptophysin (markers for motor neuron axons and terminals, respectively). Extended-focus images collected by confocal microscopy

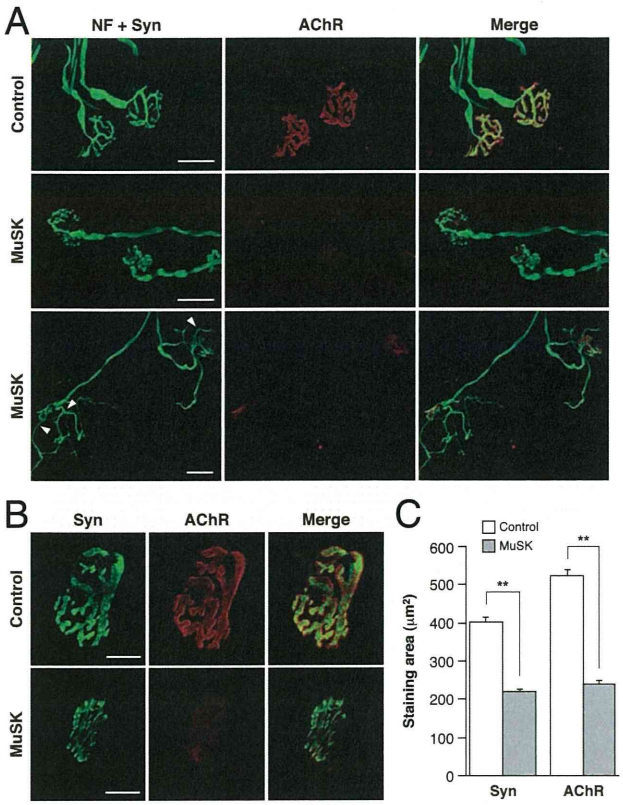

Figure 2. Disorganization of both presynaptic and postsynaptic structures in MuSK-injected mice. **A:** Whole-mount staining of NMJs from soleus muscles. Axons and nerve terminals (green) were stained with anti-neurofilament and anti-synaptophysin antibodies (NF + Syn), and AChRs (red) were labeled with rhodamine-BTx. Some NMJs with axon sprouts were observed in MuSK-injected mice (**arrowheads**). Scale bars: 30 μm. **B:** Soleus muscle nerve terminals were stained with anti-synaptophysin (green) and AChRs were stained with rhodamine-BTx (red). **C:** Synaptophysin and rhodamine-BTx-stained areas decreased to 54.8% and 45.6% of control levels, respectively, in MuSK-injected mice. Scale bars: 20 μm. Data are expressed as means ± SEM from ≥30 NMJs of each mouse (n = 3 mice/group). $^{**}P < 0.01$ versus control (t-test).

were recorded and used for quantitative structural analysis. Accordingly, areas of AChR-clustering and of apposing nerve terminals of NMJs were significantly smaller in soleus muscles of MuSK-injected mice (n = 109 NMJs from three mice), compared with controls (n = 126 NMJs from three mice) (Figure 2, A–C). Furthermore, the density of AChR clustering at NMJ postsynaptic membranes was reduced in soleus and other muscles of MuSK-injected mice, compared with control mice, as evidenced by the intensity of BTx at NMJs (Figure 2, A and B). In addition, axon sprouting, with or without the remnants of nerve terminals, was prominent at the NMJs of MuSK-injected mice (Figure 2A). These results are consistent with the axon outgrowth and reduced AChR clustering observed in other animal models of MuSK-MG.[8,23,24] These results also indicate that MuSK is required by mature NMJs for maintenance of AChR clustering at the postsynaptic membrane and apposing motor terminals. Because MuSK is expressed in skeletal muscle but not in motor neurons,[25] MuSK likely acts via retrograde signals to affect presynaptic NMJ structures.

Changes in Three-Dimensional Structures of the NMJ Subneural Apparatus

Using SEM, we studied the three-dimensional organization of the subneural apparatus at NMJs in tibialis anterior muscles after removing presynaptic terminals and connective tissues.[18] In control mice, the subneural apparatus consisted of complex labyrinthine postsynaptic gutters, approximately 0.9 to 2.8 μm in width, containing numerous slit-like junctional folds. In MuSK-injected mice, however, the subneural apparatus had shallow gutters and lost both labyrinthine structures and formerly prominent slit-like junctional folds (Figure 3A). TEM observations made in diaphragm muscles revealed that synaptic folds underneath motor terminals underwent a pronounced loss in MuSK-injected NMJs, compared with control mice (Figure 3, B and C). Of note, the synaptic membrane was well preserved in MuSK-injected animals (Figure 3B), and we observed no complement-mediated destruction of synaptic structures.[26] These data indicate that MuSK is required for the maintenance of the subneural apparatus and that the reduction of synaptic folds in MuSK-injected mice likely impaired synaptic transmission and caused muscle weakness in these animals.

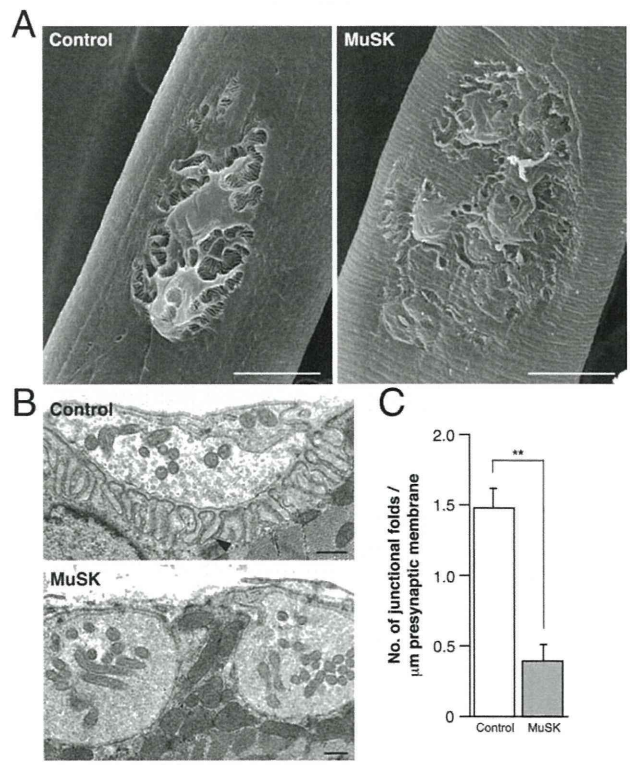

Figure 3. Disruption of NMJ ultrastructure in MuSK-injected mice. **A:** Complex synaptic gutters containing numerous slit-like junctional folds were observed by SEM in NMJs of control tibialis anterior muscle. Synaptic gutter flattening and a decreased number of slit-like junctional folds were observed in NMJs of MuSK-injected mice. Scale bars: 15 μm. **B:** Evenly distributed junctional folds (**arrowhead**) of comparable depth were observed in controls via TEM. Loss of junctional folds was observed in MuSK-injected mice. Scale bars: 500 nm. **C:** Junctional fold densities were significantly decreased in MuSK-injected mice. Data are expressed as means ± SEM from ≥10 NMJs of each mouse (n = 3 mice/group). $^{**}P < 0.01$ versus controls (t-test).

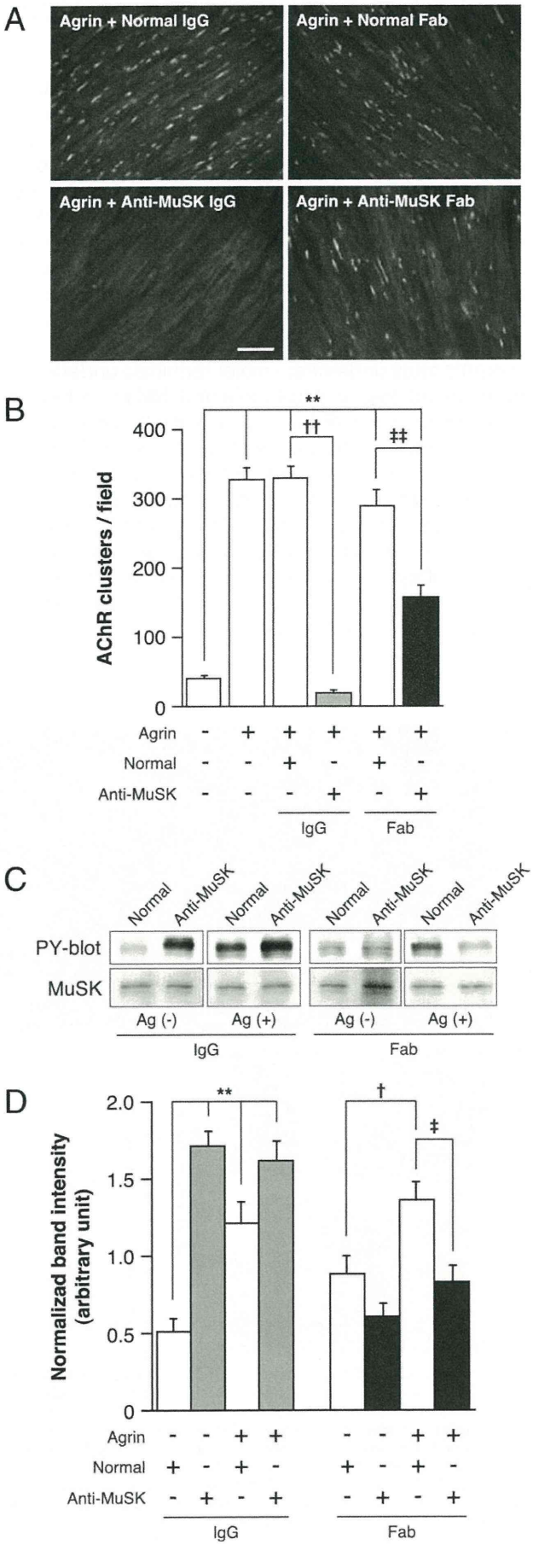

Both Divalent and Monovalent MuSK IgG Perturb MuSK Signaling in C2C12 Myotubes

Because our histological studies demonstrated that MuSK Abs caused EAMG without complement activation, we next tested MuSK Abs in sera from MuSK-injected mice for the ability to interfere with MuSK function *in vitro*. Agrin has been shown to induce the clustering of AChRs in C2C12 myotubes after autophosphorylation by MuSK.[27] When agrin and purified IgG antibodies from the sera of MuSK-injected mice were added to C2C12 myotubes, there was a significant reduction in the marked AChR clustering observed in the presence of purified IgG antibodies from normal sera (Figure 4, A and B). Because inhibition of MuSK signaling by MuSK Abs might have inhibited AChR clustering on C2C12 cells, we analyzed the effect of these antibodies on MuSK phosphorylation. However, MuSK-IgG antibodies induced tyrosine phosphorylation of MuSK in the absence of agrin, and these antibodies did not inhibit activation by agrin (Figure 4, C and D), as described previously,[7,28] suggesting that the divalent MuSK Abs altered a downstream pathway instead of inhibiting MuSK signaling directly.

Next, we generated monovalent Fab fragments of MuSK-IgG antibodies by papain digestion to determine whether they were sufficient to block MuSK signaling in C2C12 cells. Although monovalent Fab fragments of MuSK-IgG antibodies did not activate autophosphorylation of MuSK in the absence of agrin (Figure 4, C and D), these Fab fragments significantly inhibited agrin-induced AChR clustering and MuSK phosphorylation (Figure 4, A–C). These results indicate that monovalent MuSK Abs can block MuSK function *in vitro*.

Neuromuscular Transmission Is Impaired in MuSK-Injected Mice

We performed electrophysiology experiments to determine the effect of MuSK Abs on neuromuscular transmission in mature NMJs. First, we performed EMG experiments in the gastrocnemius muscles of MuSK-injected

Figure 4. Inhibition of agrin-induced MuSK function in cultured myotubes by anti-MuSK IgG and Fab fragments. **A:** C2C12 myotubes were treated with either normal IgG/Fab (10 μg/mL) or anti-MuSK IgG/Fab (10 μg/mL) for 30 minutes and then were incubated with 1 nmol/L agrin for 16 hours. AChR clusters were labeled with Alexa Fluor 594-BTx. Scale bar = 100 μm. **B:** The number of AChR clusters decreased significantly in anti-MuSK IgG or Fab-treated myotubes. Quantification was performed on six randomly selected fields from each of four experiments, and data are expressed as means ± SEM. $^{**}P < 0.01$ versus no treatment; $^{\dagger\dagger}P < 0.01$ versus treatment with agrin + normal IgG; $^{\ddagger\ddagger}P < 0.01$ versus treatment with agrin + normal Fab (analysis of variance). **C:** C2C12 myotubes were treated with either normal IgG/Fab or anti-MuSK IgG/Fab for 30 minutes. Half of the myotube cultures were then treated with 1 nmol/L agrin (Ag) for 30 minutes. Cell extracts were immunoprecipitated with MuSK antibody and immunoblotted with anti-phosphotyrosine (PY-blot) and anti-MuSK. **D:** Divalent anti-MuSK IgG treatment induced MuSK phosphorylation in the absence of agrin, but treatment with monovalent anti-MuSK Fab significantly inhibited agrin-induced MuSK phosphorylation. Band intensities of the PY-blot were normalized to total MuSK. Data are expressed as means ± SEM from three experiments. $^{**}P < 0.01$ versus treatment with normal IgG; $^{\dagger}P < 0.05$ versus treatment with normal Fab; $^{\ddagger}P < 0.05$ versus treatment with agrin + normal Fab (analysis of variance). Control: open symbols; MuSK: filled symbols.

mice with severe muscle weakness. Repetitive stimulation at 3 Hz elicited a declining CMAP response reminiscent of that observed in MG patients, whereas the CMAPs of control mice exhibited no such decline in response (Figure 5A). CMAP amplitude declined by an average of 25.8 ± 3.2% (n = 10) in MuSK-injected mice (Figure 5B). These results indicate that a failure of neuromuscular transmission was the likely cause of muscle weakness in MuSK-injected mice.

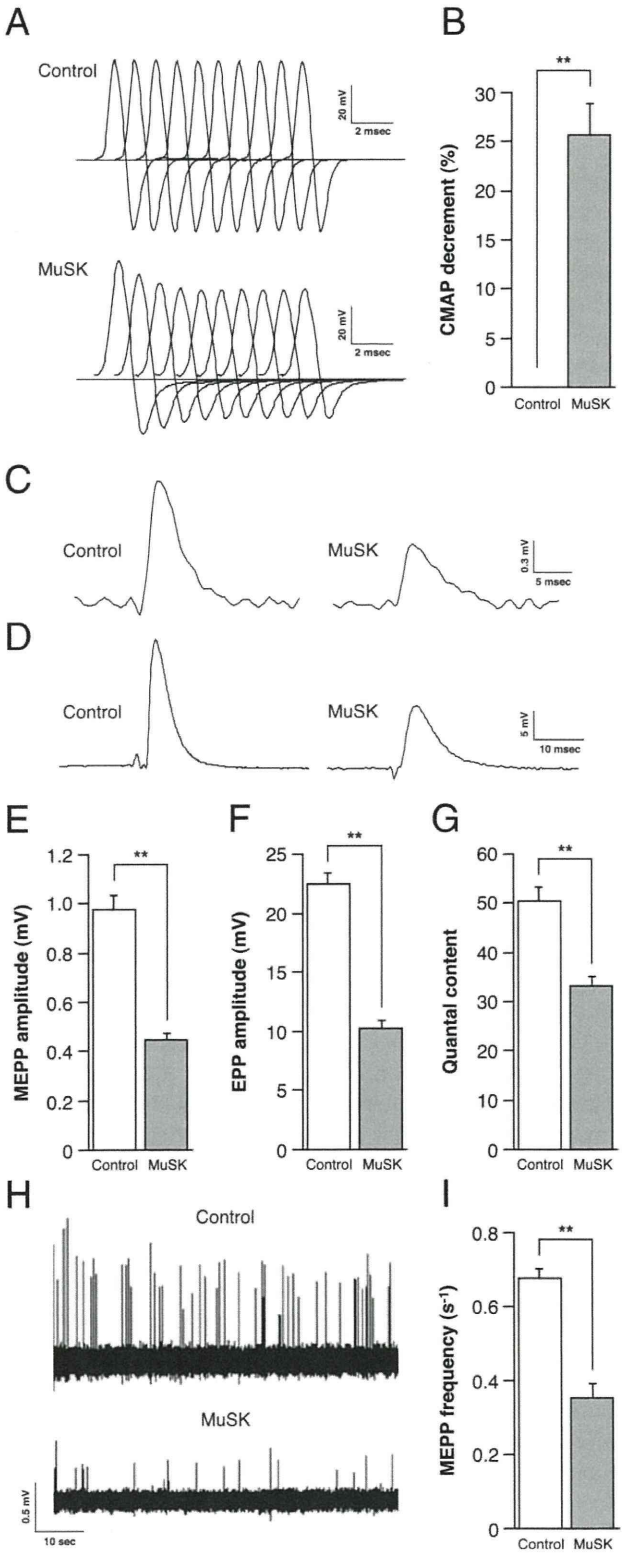

Next, we analyzed the MEPPs and EPPs of MuSK-injected mice via intracellular recordings from muscle fibers of excised hemi-diaphragms.[17,29] No significant difference was observed in resting membrane potential between control mice (−64.1 ± 0.96 mV) and MuSK-injected mice (−65.4 ± 1.33 mV). In MuSK-injected mice, both MEPP and EPP amplitudes (MEPP, 0.45 ± 0.03 mV; EPP, 10.2 ± 0.67 mV; n = 47 NMJs in 4 mice) were significantly decreased, compared with controls (MEPP, 0.98 ± 0.06 mV; EPP, 22.4 ± 0.92 mV; n = 63 NMJs in 3 mice) (Figure 5, C–F). A decrease in EPP amplitude could result either from fewer transmitter quanta being released by a single nerve impulse or from a smaller effect of individual quanta.[30] In addition to the decreased MEPP amplitude, which indicates a smaller postsynaptic effect, the mean quantal content (ie, the steady-state number of quanta released by a single nerve impulse under stimulation at 0.7 Hz) of MuSK-injected diaphragms was also decreased, falling to 33.3 ± 1.78 (or 66.2% of the normal value, 50.3 ± 2.92) (Figure 5G). Taken together, these two effects could result in decreased EPP amplitude, leading to CMAP amplitude decrements.

In addition to the decrease in stimulation-dependent quantal release, MuSK-injected mice (0.35 ± 0.04/s; n = 48 NMJs in 4 mice) exhibited a 52% reduction in spontaneous release, as observed in MEPP frequency, compared with controls (0.67 ± 0.02/s; n = 61 NMJs in 4 mice) (Figure 5, H and I). Because MuSK protein injection resulted in decrease in MEPP amplitude due to the loss of AChR clusters, we could not exclude the possibility that some of the emerging MEPPs were undetectable by our method. However, these results might indicate a low probability of spontaneous quantal ACh release resulting from a presynaptic defect in MuSK-injected mice, as described previously.[31,32]

MuSK-EAMG Is Inducible in Other Complement-Deficient Strains of Mice

A/WySnJ mice exhibit a significant loss of mature B cells due to the B-cell maturation defect-1 (*Bcmd*-1) mutant allele of B-cell-activating factor receptor (*BAFF-R*), and are genetically prone to develop B cell-mediated autoimmunity.[33,34] [*BAFF-R* has since been reclassified as tumor necrosis factor receptor superfamily, member 13c

Figure 5. Impairment of neuromuscular transmission after MuSK injection. **A:** Representative EMG traces during repetitive nerve stimulation. MuSK-injected mice exhibited a decremental CMAP amplitude response, consistent with MG. **B:** MuSK-injected mice exhibited significant CMAP decline (mean, 25.8 ± 3.2%). n = 3, control; n = 10, MuSK-injected. Representative MEPP (**C**) and EPP (**D**) traces from diaphragm muscles. Mean amplitudes of both MEPPs (**E**) and EPPs (**F**), as well as mean quantal release by nerve stimulation (**G**), were decreased in MuSK-injected mice to 45.9%, 45.5%, and 66.2% of control values, respectively. Data are expressed as means ± SEM from ≥10 NMJs of each mouse (n = 3, control; n = 4, MuSK-injected). **H:** Representative MEPP recordings from diaphragm muscles. **I:** MEPP frequencies were decreased to 52.0% of control levels in MuSK-injected mice. Data are expressed as means ± SEM from ≥10 NMJs of each mouse (n = 4 mice/group). $^{**}P < 0.01$ versus controls (t-test).